Radiotherapy and Oncology 162 (2021) 140–149

Contents lists available at ScienceDirect

Radiotherapy and Oncology

journal homepage: www.thegreenjournal.com

Original Article

Chemical exchange saturation transfer MRI in central nervous system tumours on a 1.5 T MR-Linac

Rachel W. Chan [a,*], Liam S.P. Lawrence [b], Ryan T. Oglesby [a,b], Hanbo Chen [c], James Stewart [c], Aimee Theriault [c], Mikki Campbell [c], Mark Ruschin [c], Sten Myrehaug [c], Eshetu G. Atenafu [d], Brian Keller [d], Brige Chugh [c,e], Scott MacKenzie [c], Chia-Lin Tseng [c], Jay Detsky [c], Pejman J. Maralani [f], Greg J. Czarnota [a,b,c], Greg J. Stanisz [a,b,g], Arjun Sahgal [c], Angus Z. Lau [a,b]

[a] Physical Sciences Platform, Sunnybrook Research Institute, Toronto, Canada; [b] Department of Medical Biophysics, University of Toronto, Toronto, Canada; [c] Department of Radiation Oncology, Sunnybrook Health Sciences Centre, University of Toronto, Toronto, Canada; [d] Department of Biostatistics, University Health Network, University of Toronto, Toronto, Canada; [e] Department of Physics, Ryerson University, Toronto; [f] Department of Medical Imaging, University of Toronto, Sunnybrook Health Sciences Centre, Toronto, Canada; [g] Department of Neurosurgery and Pediatric Neurosurgery, Medical University of Lublin, Lublin, Poland

ARTICLE INFO

Article history:
Received 17 March 2021
Received in revised form 6 July 2021
Accepted 8 July 2021
Available online 17 July 2021

Keywords:
MR-Linac
Radiation therapy
Treatment monitoring
MRI guided therapy
Quantitative MRI
Chemical exchange saturation transfer

ABSTRACT

Purpose: To describe the implementation and initial results of using Chemical Exchange Saturation Transfer (CEST) for monitoring patients with central nervous system (CNS) tumours treated using a 1.5 tesla MR-guided radiotherapy system.

Methods: CNS patients were treated with up to 30 fractions (total dose up to 60 Gy) using a 1.5 T Elekta Unity MR-Linac. CEST scans were obtained in 54 subjects at one or more time points during treatment. CEST metrics, including the amide magnetization transfer ratio (MTR_{Amide}), nuclear Overhauser effect (NOE) MTR (MTR_{NOE}) and asymmetry, were quantified in phantoms and CNS patients. The signal was investigated between tumour and white matter, across time, and across disease categories including high- and low-grade tumours.

Results: The gross tumour volume (GTV) exhibited lower MTR_{Amide} and MTR_{NOE} and higher asymmetry compared to contralateral normal appearing white matter. Signal changes in the GTV during fractionated radiotherapy were observed. There were differences between high- and low-grade tumours, with higher CEST asymmetry associated with higher grade disease.

Conclusion: CEST MRI using a 1.5 T MR-Linac was demonstrated to be feasible for *in vivo* imaging of CNS tumours. CEST images showed tumour/white-matter contrast, temporal CEST signal changes, and associations with tumour grade. These results show promise for the eventual goal of using metabolic imaging to inform the design of adaptive radiotherapy protocols.

Magnetic resonance imaging (MRI) in clinical practice has expanded from a diagnostic tool to one of image guidance. This includes the integration of MRI into radiotherapy, for which a number of MR-guided radiotherapy systems have emerged [1,2]. The Elekta Unity MR-Linac is a new system that combines a linear accelerator with an MR scanner [3,4], employing a magnetic field strength of 1.5 tesla to enable high-resolution diagnostic-quality images at each radiation treatment fraction. The ability to perform real-time MR guidance [1] offers new opportunities for response assessment and personalized treatment in radiotherapy. Various clinical applications of the MR-Linac [5–9] have used soft-tissue MRI contrast for target volume planning and for the sparing of organs at risk. In addition, advanced quantitative MRI sequences have been explored to obtain microstructural information throughout treatment on MR-guided radiotherapy systems [10,11], which could potentially be used to identify regions for dose intensification [12].

Chemical exchange saturation transfer (CEST) [13] MRI is capable of acquiring metabolic information and is sensitive to low (millimolar) metabolite concentrations. Amide proton transfer (APT) CEST [14,15], which is based on the exchange of protons in amide bonds such as those of proteins and peptides, has been shown to predict therapeutic response in glioblastoma (GBM) [16–18], discriminate between different central nervous system (CNS) tumour types [19–22] and grades [19], distinguish radiation necrosis from tumour [23] and differentiate pseudoprogression from true progression [24]. *In vivo* CEST was traditionally limited to MRI field strengths of 3 T and 7 T [17,18,25,26]. Recently, our

* Corresponding author at: 2075 Bayview Ave., S6-05, Toronto, ON M4N 3M5, Canada.
E-mail address: rchan@sri.utoronto.ca (R.W. Chan).

https://doi.org/10.1016/j.radonc.2021.07.010
0167-8140/

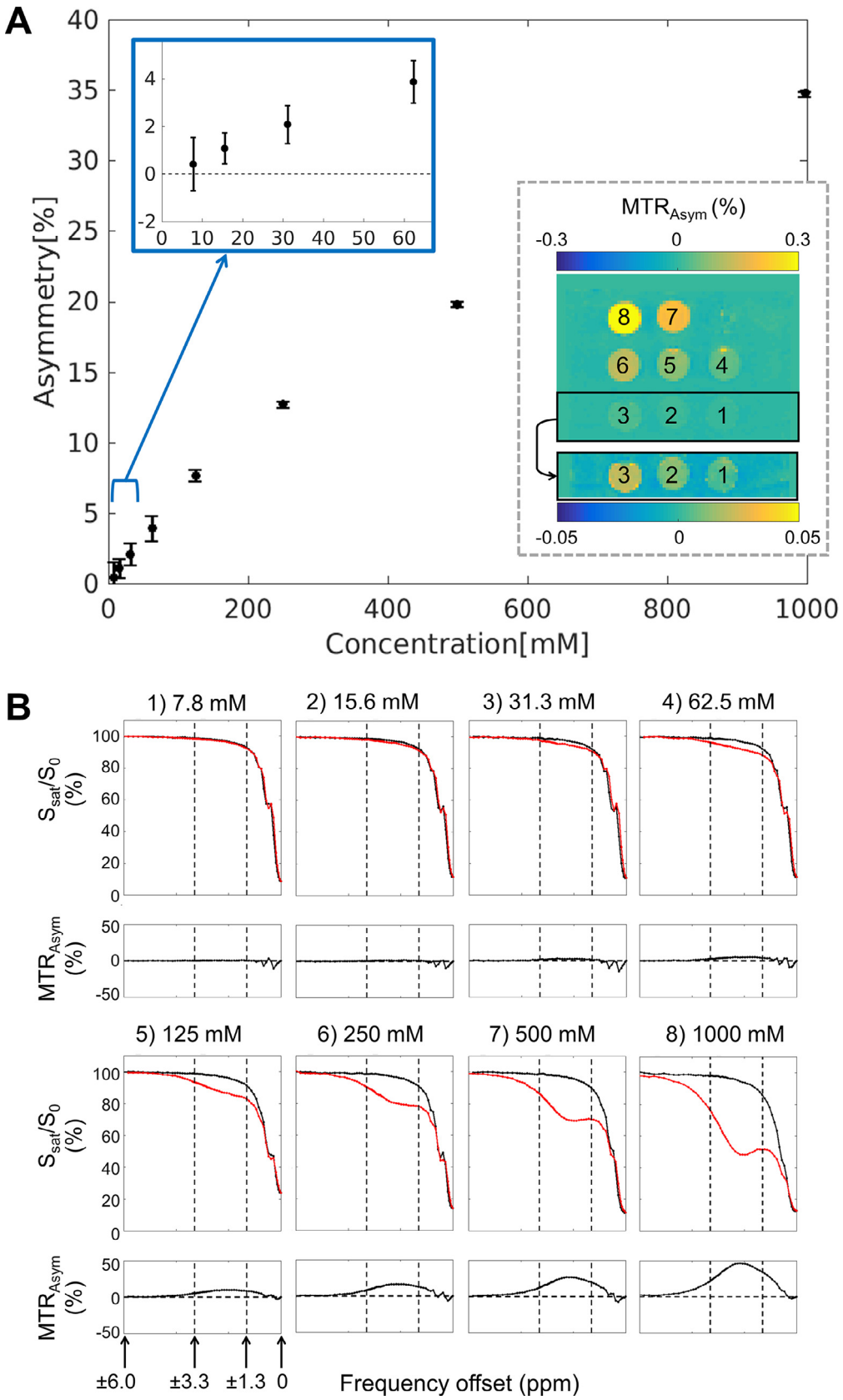

Fig. 1. CEST Phantom Experiment on the MR-Linac: (A) Mean CEST asymmetry values (with standard deviation represented by errorbars) are plotted for eight ammonium chloride concentrations, along with the asymmetry map. ROIs are labeled 1–8, corresponding to increasing NH_4Cl concentrations. Map intensities outside the tubes are from the water in which the phantom tubes were immersed to reduce susceptibility effects. (B) Corresponding z-spectra are shown. Signal amplitudes from the positive (red) and negative (black) frequency offsets are plotted with differences representing the MTR asymmetry at each offset.

Table 1
Patient Characteristics: Patient characteristics are shown for 54 CNS patients included in this study. Clinical details for the subset of 28 GBM patients are also included. All brain metastases were cavities.

CNS patients (n = 54)	
Age (years)	
Median	54
Range	26–81
Gender	
Female	25 (46.3%)
Male	29 (53.7%)
Diagnosis	
GBM	28 (51.9%)
Astrocytoma	10 (18.5%) (Gr.II: 5/Gr.III: 4/not assessed: 1)
Brain metastasis	7 (13.0%)
Meningioma	4 (7.4%)
Oligodendroglioma	3 (5.6%)
Ependymoma	1 (1.9%)
Schwannoma	1 (1.9%)
WHO Grade	
I	3 (5.6%)
II	8 (14.8%)
III	6 (11.1%)
IV	28 (51.9%)
N/A	9 (16.7%)
Tumour location by lobe	
Frontal	15 (27.8%)
Temporal	13 (24.0%)
Parietal	5 (9.2%)
Occipital	3 (5.6%)
Cerebellar	2 (3.7%)
Thalamus	2 (3.7%)
Ventricle	2 (3.7%)
Other	6 (11.1%)
Multiple lobes	6 (11.1%)
Tumour location by hemisphere	
Left	23 (42.6%)
Right	22 (40.7%)
Bilateral	6 (11.1%)
N/A or unknown	3 (5.6%)
GBM patients (n = 28)	
Age (years)	
Median	57
Range	26–81
Gender	
Female	11 (39.3%)
Male	17 (60.7%)
Resection status	
Gross total resection (GTR)	12 (42.9%)
Subtotal resection (STR)	8 (28.6%)
Biopsied	8 (28.6%)
IDH mutation status	
Wild Type	27 (96.4%)
Mutant	1 (3.6%)
MGMT methylation status	
Methylated	11 (39.3%)
Unmethylated	12 (42.9%)
N/A or unknown	5 (17.9%)

group implemented CEST on a 1.5 T clinical scanner using a pulsed saturation scheme [27]. Consistent with findings at higher field strengths [16–18], we showed associations between treatment response and CEST metrics measured during chemoradiation in GBM patients [28]. However, CEST has not been implemented on MR-guided radiotherapy systems, where it could be used directly to inform the adaptation of radiotherapy plans based on observed biological changes of the tumour. This study was the first to investigate the use of *in vivo* CEST on a hybrid MR-Linac system and extends previous work on diagnostic MR scanners at 1.5 T [27,28] and 3 T [7–9]. We demonstrate that CEST images can be successfully obtained within the clinical workflow of MR-Linac treatment in CNS patients.

The aims of this study were to describe the implementation of CEST on a 1.5 T MR-Linac (Unity, Elekta AB, Stockholm, Sweden), including phantom validation, and to present initial results in CNS patients evaluating (1) cohort differences between the gross tumour volume (GTV) and contralateral normal appearing white matter (cNAWM) regions, (2) cohort signal changes during treatment, and (3) the association between CEST signals and tumour grade.

Materials and methods

Phantom experiment

To evaluate the sensitivity of CEST detection, mixtures of ammonium chloride (NH_4Cl; concentrations {7.8, 15.6, 31.3, 62.5, 125, 250, 500, 1000} mM) doped with 1.0 mM copper sulfate pentahydrate ($CuSO_4{\cdot}5H_2O$) were prepared and imaged using a single-slice CEST sequence on the MR-Linac with the MR parameters shown in Supplementary Fig. S1 (same as *in vivo* scans). The 50 mL tubes containing the mixtures were arranged in a grid fixture and immersed in water. The tubes were oriented parallel to the B_0 field of the scanner and imaged axially.

Study design and image acquisition

All imaging for CNS patients was performed on the 1.5 T MR-Linac, where patients were treated with radiation. Patients with GBM and grades II/III astrocytomas received concurrent chemotherapy. Patients with metastasis received prior chemotherapy and those with oligodendrogliomas received chemotherapy either during or post-radiation. All patients were enrolled in the MOMENTUM study (ClinicalTrials.gov, identifier: NCT04075305) [29]. The study was approved by the institutional research ethics board and informed consent was obtained. The anterior and posterior coils, each consisting of four channels (element size = 440 × 1 28 mm) [30], were used for imaging. Patients were immobilized using thermoplastic mask (Orfit Industries, Wijnegem, Belgium) and in most cases, positioned in the bore using a fixed indexing location on the treatment couch. Depending on the disease, there were a different total number of fractions. GBM patients were either treated with 60 Gy in 30 fractions or, in 8 cases, 40 Gy in 15 fractions. Brain metastasis cavities were treated with 27.5 Gy in 5 fractions. An adapt-to-position workflow was used for daily planning [31] to account for translations in patient positioning. T_1-weighted (T1w) and T_2-weighted Fluid-Attenuated Inversion Recovery (FLAIR) scans were taken on each day of treatment. CEST images were acquired on the third day of the five-day week [32] after dose delivery (i.e., during post-beam time immediately after the radiation treatment), between fractions 1 and 30. The CEST imaging pulse sequence was previously developed and validated for a Philips 1.5 T Ingenia [27,28], with the source code recompiled for the MR-Linac. All MR-Linac imaging parameters, including CEST, B_0, and B_1 mapping scans, are included in Supplementary Fig. S1.

The single axial CEST slice was prescribed by identifying the superior/inferior (SI) "z" location of the greatest axial tumour diameter at the first CEST scan. At subsequent time points, CEST scans were, in most cases, acquired at the same z-location relative to the magnet. Scan sessions where the imaged region had a slice offset greater than 5 mm (i.e., the CEST slice thickness) were excluded from the analysis. This processing step accounts for inter-session rotations or translations of the patient anatomy, but not internal deformations from changes in edema or mass effect.

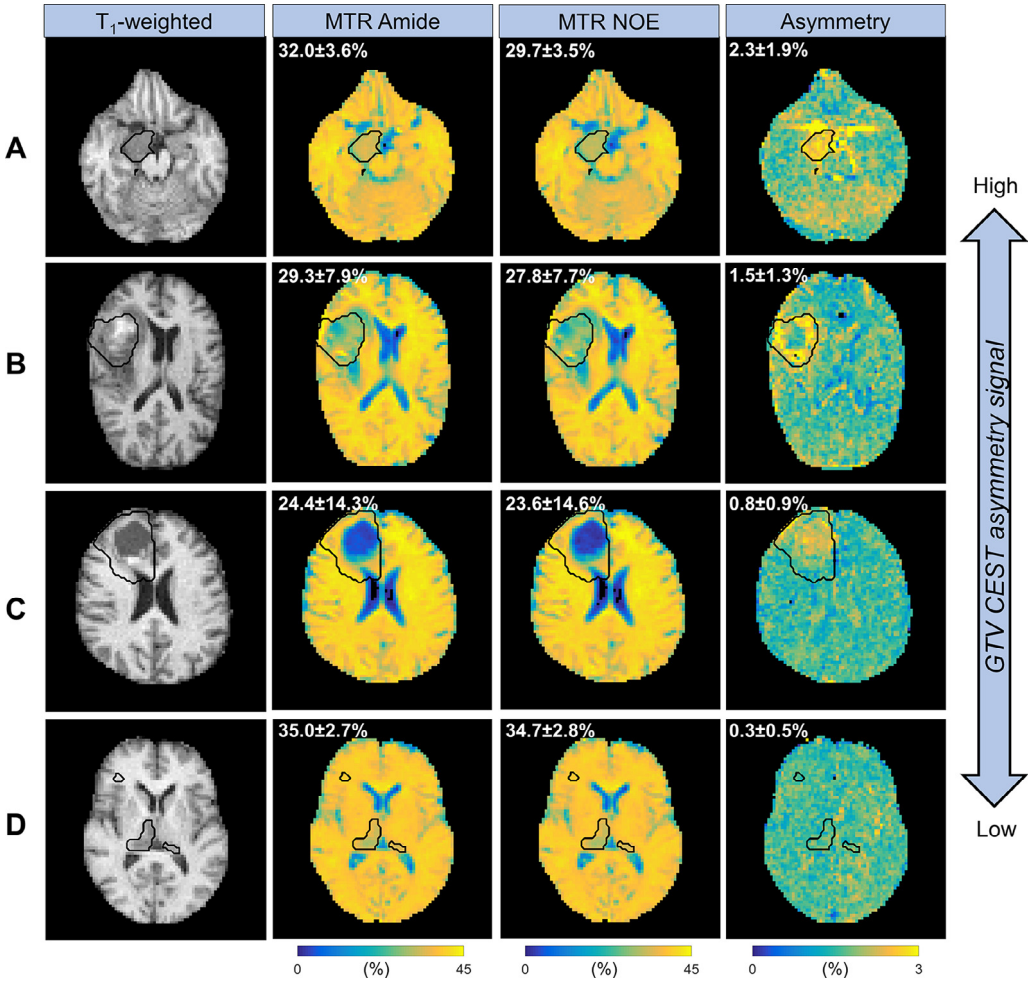

Fig. 2. MR-Linac CEST maps in CNS patients: Selected CEST parameter maps (MTR_{Amide}, MTR_{NOE} and asymmetry), ordered from the highest to lowest median GTV (black contour) asymmetry values, are displayed for examples of (A) meningioma, (B) GBM, (C) oligodendroglioma and (D) astrocytoma. T_1-weighted images are shown for anatomical reference. Mean values and standard deviations over the GTV are shown.

The procedure for slice offset estimation involves rigidly registering all daily T1w images to the first CEST time point. The resulting transformation matrix was applied to each CEST slice, mapping the slice to the coordinate system of the first time point. At each (x,y) location, the slice offset $\Delta z(x,y)$ was computed and the median superior-inferior slice offset over the clinical target volume (CTV), denoted Δz_{SS}, was determined for each scan session, as shown in Supplementary Fig. S2. All image analysis used MATLAB R2018b (The MathWorks, Natick, MA).

Image processing

The CEST magnetization transfer ratio (MTR) asymmetry, MTR_{Amide} and MTR_{NOE} metrics were quantified:

$$MTR_{Amide} = \frac{S(ref) - S(f)}{S(ref)}$$

$$MTR_{NOE} = \frac{S(ref) - S(-f)}{S(ref)}$$

$$Asymmetry = \frac{S(-f) - S(f)}{S(ref)}$$

Where the signal, $S(f)$, is computed as $\frac{1}{\Delta f}\sum_{f1}^{f2} S(f)$ over a range of frequencies $\Delta f = |f2 - f1|$ around f = 3.5 ppm (or 224 Hz at 1.5 T) for the CEST amide peak and $-f$ for the nuclear Overhauser effect (NOE) aliphatic peak. $S(ref)$ is the signal from the reference image (acquired far off-resonance at a frequency offset of 100,000 Hz, or equivalently, 1566 ppm at 1.5 T, to ensure that there is no saturation of the CEST species for the signal normalization). The three metrics used for CEST quantification provide distinct information. The magnetization transfer ratio (MTR) measures the sum of all saturation effects (at the respective amide and NOE frequency offsets on each side of the z-spectra), and is a non-quantitative metric that includes CEST and other non-CEST effects (e.g., direct water saturation and magnetization transfer contrast). The asymmetry, or the difference between MTR_{Amide} and MTR_{NOE}, is a semi-quantitative metric that removes the direct water saturation and MT effects. Scans that were acquired with 1.5 and 3 μT were interpolated to 2.5 μT. Correction for the B_0 and B_1 inhomogeneity was applied on a voxelwise basis before computing the CEST metrics [27,28]. Each parameter was quantified between 2 and 4 ppm in human subjects. In phantoms, the quantification was done between 1.3 and 3.3 ppm around the NH_4Cl resonance of 2.3 ppm.

The gross tumour volume (GTV) was contoured as part of treatment planning using post-gadolinium T_1-weighted images and T_2-weighted FLAIR images. The GTV was propagated to each daily fraction by rigidly co-registering the CT simulation image to the (non-contrast) MR-Linac T_1-weighted image using FSL FLIRT [33]. HD-BET [56] was used to extract the brain and FSL FAST [33] was

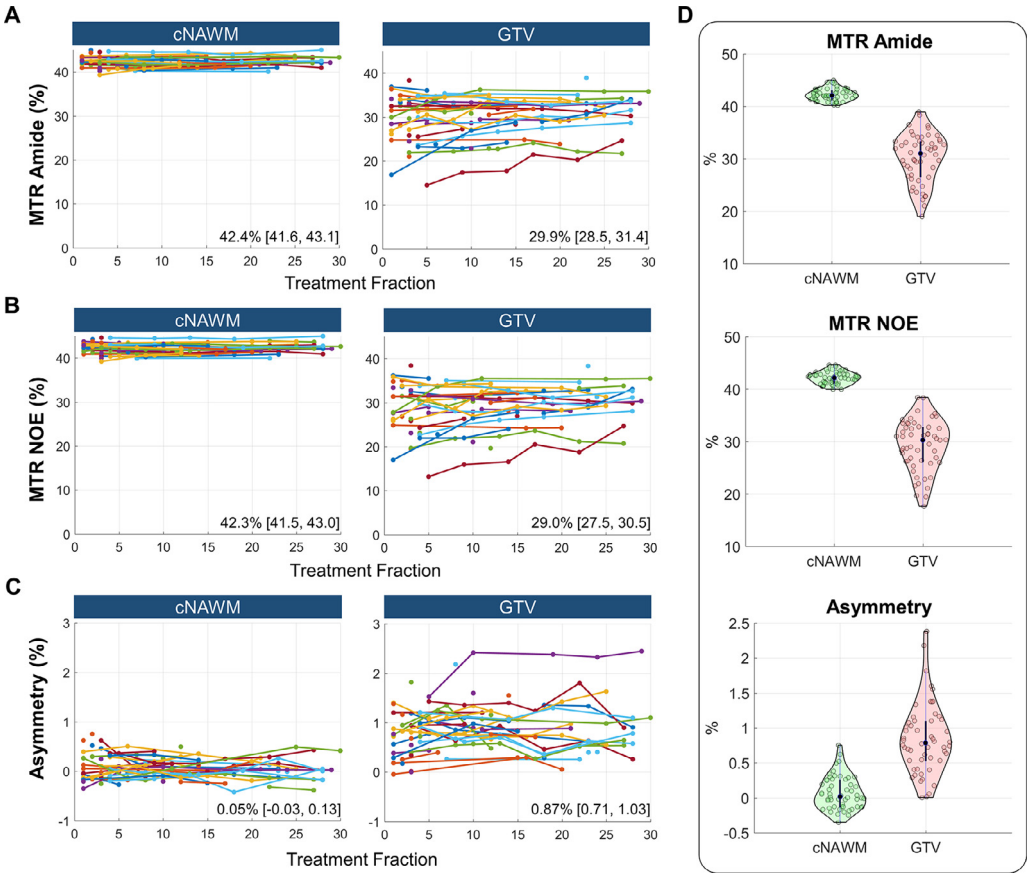

Fig. 3. CEST values in GTV and cNAWM: CEST parameter values with respect to treatment fraction are displayed for (A) MTR_{Amide}, (B) MTR_{NOE}, and (C) asymmetry, for each ROI (cNAWM and GTV). The number of scan sessions differed between patients. Each point represents a single scan session and connected points are of the same subject, for n = 54 subjects. The overall means and confidence intervals [2.5%, 97.5%] from mixed effects modelling are shown for each plot. (D) Summary violin plots are shown, after taking the median across time, for cNAWM and GTV.

used to automatically segment the white matter regions, followed by manual selection of contralateral normal appearing white matter (cNAWM).

For the analysis of tumour grade, necrotic regions and resection cavities, denoted "NR" regions, were removed from the GTV to generate an additional ROI, denoted "GTV-minus-NR", that represents the GTV regions after subtraction of the necrotic regions or resection cavities. The NR regions were manually drawn by a neuroradiologist with 10 years of experience, based on the co-registered pre- and post-contrast T_1-weighted images that corresponded to the imaged CEST slice. The post-contrast images were acquired on a diagnostic scanner that was used for radiation planning, prior to the treatment. The necrotic regions were drawn at a higher image resolution (voxel size: $1 \times 1 \times 5$ mm^3), then downsampled to the CEST resolution (voxel size: $2.5 \times 2.5 \times 5.0$ mm^3).

Comparisons and statistical analysis

Categorical variables included the diagnosis and WHO grade. Continuous variables included the median CEST signals (MTR_{Amide}, MTR_{NOE} and asymmetry). Three comparisons were performed:

1) GTV vs. cNAWM: Mixed effects modelling was used to assess differences in the median CEST signals (MTR_{Amide}, MTR_{NOE} and asymmetry) between the two ROIs (GTV and cNAWM) over the entire cohort, using the ROI as a fixed effect and subject as a random effect.

2) Temporal changes: To determine if there were cohort changes in the CEST parameters over time, the median signals within the GTV over treatment fractions were assessed using mixed effects modelling, with treatment fraction modelled as a fixed effect (continuous variable) and subject as a random effect. Individual changes were assessed in those patients with the most stable positioning over time (Δz_{ss} < 1.5 mm).

3) Tumour types and grade: MTR_{Amide}, MTR_{NOE} and asymmetry values were compared between high- (grades III, IV) and low-grade (grades I, II) tumours, where differences were assessed with both Wilcoxon rank-sum tests and univariable logistic regression for the first treatment fraction of each patient. These were assessed in each of two ROIs (the GTV with and without necrotic/resected regions), for each CEST parameter, and for the glioma-only and CNS cohorts. The medians for each disease category (e.g., GBM, astrocytomas, brain metastasis cavities) were also computed.

Statistical analysis used R (v4.0.2x64: R Core Team (2020), Vienna, Austria). The threshold for statistical significance was 0.05 for all hypothesis testing, with unadjusted p-values reported for all comparisons.

Results

Fig. 1 shows the results of phantom experiments, including asymmetry maps and plots of the z-spectra at each concentration. The MTR asymmetry increased with increasing concentration, from 0.41 ± 0.18% (mean ± SD within ROI) for the lowest NH_4Cl concentration (7.8 mM) to 34.7 ± 1.1% for the highest concentration

(1000 mM). This trend in asymmetry supports the hypothesis that CEST MRI is feasible on a 1.5 T MR-Linac.

Patient characteristics are detailed in Table 1. CNS tumour types consisted of gliomas (WHO grades I–IV), resected brain metastases and benign tumours. Two scans were incomplete and were excluded, as were 10 scans where the median positioning error across the CTV exceeded 5 mm. The distribution of positioning errors is shown in Supplementary Fig. S2. After exclusion, there were 129 scan sessions (n = 54 patients) included in our analysis. In addition to a variable total number of fractions between patients (e.g., 27.5 Gy in 5 fractions for brain metastasis cavities, compared to 60 Gy in 30 fractions or 40 Gy in 15 fractions for GBM), only a subset of fractions were delivered on the MR-Linac (median of 24 fractions per subject). Reasons include (i) patients having part of their radiation treatment on another (non-MR-Linac) machine, (ii) MR-Linac downtime (including both unexpected downtime such as that required by replacement of hardware and expected downtime such as public holidays), and (iii) subjects who declined post-beam imaging for a particular scan session. The median number of CEST scans was two sessions per subject.

MTR_{Amide}, MTR_{NOE} and asymmetry maps in CNS tumours are shown in Fig. 2, demonstrating a range of GTV values consisting of both high asymmetry (=2.3% ± 1.9% as found in a meningioma, Fig. 2A) and low asymmetry values (=0.3 ± 0.5%, as found for an astrocytoma, Fig. 2D). In Fig. 3, plots of each CEST parameter value (MTR_{Amide}, MTR_{NOE}, asymmetry) versus treatment fraction in GTV and cNAWM are shown. The CEST contrast over the entire cohort was significantly different between GTV and cNAWM (p < 0.001 for all parameters). Violin plots comparing the median value across time between GTV and cNAWM are shown in Fig. 3D for each parameter.

Analysis of signal changes over treatment fractions by mixed effects modelling over all 54 subjects and 129 scan sessions combined showed an increasing trend in MTR_{Amide} and MTR_{NOE} parameters (p < 0.05 for both). Asymmetry showed no significant association with fraction. CEST signal changes in individual subjects were found in the subset of patients with the most stable slice positioning (<1.5 mm across scan sessions). Additional results for the two groups (small shifts of Δz_{ss} < 1.5 mm vs. larger shifts of 1.5 mm < Δz_{ss} < 5.0 mm) are shown in Supplementary Fig. S3. CEST signal changes were found only in the group with small slice shifts, with example subjects displayed in Fig. 4. Fig. 4A shows a subject with relatively constant MTR_{Amide} and asymmetry GTV signals relative to the first time point, except for a slight increase in asymmetry between fractions 16 and 21 (p < 0.05). Pt42 in Fig. 4B shows increasing MTR_{Amide} signal over time with a decrease in asymmetry between fractions 14 and 17 (p < 0.05, using t-tests between time points). In Fig. 4C, additional ROIs were analyzed for subject Pt50. In both the GTV and ROI 1 (within the GTV), there were increasing MTR_{Amide} signals over time. There were also temporal changes outside of the GTV, as seen in ROI 2, where a decrease was found in the MTR_{Amide} signal. The similarity between the MTR_{Amide} and MTR_{NOE} signals reflected the results of our previous study [27] that compared 1.5 T and 3 T in the brain of the same healthy subject, where similar NOE and amide maps were found at 1.5 T, compared to 3 T (which had higher NOE). The repeatability coefficient (RC) and coefficient of variation (CV) for the three CEST metrics in cNAWM are also shown in Supplementary Fig. S4.

In Fig. 5A, the signals for each disease category are shown after taking the median signal across all time points for each patient. The GBM cohort (of which 27/28 were IDH1 wildtype), has the second lowest median MTR_{Amide} value of 29.5% (cohort IQR = 8.5%) and a median asymmetry of 0.91% (IQR = 0.41) after averaging over all time points. It can be seen that resected brain metastasis cavities have the lowest median MTR_{Amide} value of 28.1% (IQR = 4.6%). Grade III astrocytomas have higher asymmetry (=0.96%, IQR = 1.60%) than grade II astrocytomas (=0.34%, IQR = 0.45%). One case of ependymoma also has a relatively high asymmetry value of 0.95%.

Results comparing high- and low-grade tumours are shown in Fig. 5B for the glioma cohort. In the GTV, there were larger differences in the amide/NOE MTR values between high- and low-grade tumours (with median MTR_{Amide} = 29.6% for HG and MTR_{Amide} = 32.5% for LG, and MTR_{NOE} = 28.0% for HG and MTR_{NOE} = 31.5% for LG) compared to the GTV-minus-NR region, where differences were largely eliminated after exclusion of the necrotic regions and resection cavities, resulting in similar medians between MTR_{Amide} and MTR_{NOE} (with median MTR_{Amide} = 33.2% for HG and MTR_{Amide} = 32.5% for LG, and MTR_{NOE} = 32.1% for HG and MTR_{NOE} = 32.0% for LG). However, in the CEST asymmetry parameter, there was slightly greater separation between the two groups for GTV-minus-NR (with median asymmetry of 0.98% in HG and 0.34% for LG) compared to GTV (with median asymmetry of 0.89% for HG and 0.34% for LG). Plots for the CNS cohort are shown in Supplementary Fig. S5, with example maps of the GTV and GTV-minus-NR contours included in Supplementary Fig. S6.

Discussion

Accurate identification of which tumours are responsive to radiation treatment remains a clinical challenge. Obtaining metabolic information during treatment will improve our understanding of how CNS tumours respond to treatment. In this study, it was demonstrated that CEST imaging can be performed on a clinical 1.5 T MR-Linac in patients during radiotherapy. Images obtained in CNS tumours demonstrated (i) tumour/white-matter contrast, (ii) CEST signal changes over time and (iii) differences between high and low tumour grades. Three CEST metrics were quantified. The asymmetry has been used in numerous clinical applications of amide proton transfer [34,35], including in previous studies that investigated tumour grade [19,36]. While not quantitative, the amide/NOE MTR metrics have been shown to be useful for differentiating tumour from radiation necrosis in brain metastases [23].

CEST signal contrast was found between GTV and cNAWM over the entire cohort. This is consistent with previous studies on diagnostic scanners including at 1.5 T in GBM tumours [28] and at 3 T in brain metastases patients [37]. Analysis of signal changes in individual subjects also revealed instances of MTR_{Amide} signal changes, both increasing and decreasing, depending on the ROI analyzed. Future analyses of the CEST signals in the MR-Linac cohort can include the correlation of the cNAWM signal to therapy response [37,38], as CEST may be sensitive to tumour infiltration in apparently healthy brain tissue.

In Hong et al. [39] at 4.7 T, histogram analysis shows a decrease in the tumour APT signals (relative to pre-treatment baseline) at all time points following radiation treatment (up to 14 days post-radiation) in glioma models. In another pre-clinical study [40] with temozolomide-only treatment, a reduction in the APT ratios (normalized by the contralateral signal) is apparent following treatment in glioma mouse models, whereas the ratios in untreated controls continued to increase. In our study, changes in both directions were observed in the CEST metrics. Moreover, it was found that the trend can depend on the chosen ROI (Fig. 4C). The changes could be due in part to post-surgical effects in tumours that were partially or completely resected. Nevertheless, changes were found outside of the GTV (as in Fig. 4C, ROI 2), suggesting that analysis of peritumoural FLAIR-hyperintense regions [28,41], which are known to harbour tumour cells in gliomas [42], would be worthwhile for the evaluation of CEST signals for outcome prediction, and will be included in more comprehensive future analyses.

Joo et al. [22] found that CEST can distinguish between benign and atypical meningiomas, with atypical meningiomas having significantly greater asymmetry than benign meningiomas (2.46% vs. 1.67%; $p < 0.001$). The benign meningioma in our study, shown in Fig. 2A, had one of the highest asymmetry values (2.3 ± 1.9%), which is larger than that of the benign meningiomas from Joo et al., but was lower than their reports of atypical meningioma asymmetry. Grades II and III astrocytomas had relatively high MTR_{Amide} (median = 33.6%, IQR = 22.5%) in comparison to GBM. The lower MTR_{Amide} values in GBM demonstrated in our study compared to other tumours could be reflective of necrotic regions inherent in GBM tumours.

Lower MTR_{Amide} and MTR_{NOE} values for high-grade tumours in the GTV compared to the GTV-minus-NR region suggest that necrotic or resected regions (within the GTV) are sources of differences between high- and low-grade tumours, when included in the ROI. This is consistent with previous studies showing that radiation necrosis is associated with lower MTR_{Amide} and MTR_{NOE} values compared to active tumour [23]. Our results showed that the asymmetry was largely unaffected by the removal of necrotic regions, with slightly better separation (and lower p-values) in the glioma-only cohort between high- and low-grade tumours. The trends in asymmetry were consistent with literature reports [19,36] at field strengths higher than 1.5 T, showing increased asymmetry in high-grade tumours. As our study is exploratory, with relatively few patients in each group, two tests were investigated. For the Wilcoxon rank-sum test, the continuous outcome variables were the three CEST parameters (MTR_{Amide}, MTR_{NOE} and asymmetry) to compare between high- and low-grade cohorts. For logistic regression, the binary outcomes were the high- and low-grade categories. Both methods yielded differences in the asymmetry parameter (although without correction for multiple testing) for both GTV and GTV-minus-NR in the glioma cohort.

Significant differences in CEST metrics were found between high- and low-grade tumours, which has not previously been demonstrated at 1.5 T. These results reflect similar findings from other authors at 3 T [19,36]. Togao et al. [19] at 3 T additionally demonstrated positive correlations of the asymmetry signal to the Ki-67 labelling index, a marker of cell proliferation and to the histologically determined cell density. They found significant asymmetry differences between the low-grade (2.1 ± 0.4%) and high-grade groups (3.9 ± 1.1%). Although our results showed similar trends between high and low grades, the asymmetry values obtained were substantially lower for both categories (with asymmetry of 0.93% CI = [0.78, 1.1] for high grade and 0.59% CI = [0.13, 1.1] for low-grade tumours). Future analyses would benefit from larger sample sizes and also from correlation with histopathological features including markers of cell density and proliferation.

One of the limitations of our study is that a single slice acquisition was used to image the tumour over time. The use of automatic MR planning approaches that take into account rotations and translations would be an alternative approach for selecting the same slice compared to previous sessions. However, this may not account for tumour changes or mass effect. In future studies, using volumetric CEST imaging to cover the entire tumour [43–45] would ensure minimal sensitivity to positioning errors, and, together with 3D registration between the sessions, the same brain tissue could be followed over time for guiding 3D radiotherapy plan adaptation based on CEST MRI. Parallel imaging with CEST [46] could be explored together with improvements in the imaging hardware, including radiolucent head coils with conforming coil elements and higher channel counts [47], which could help to accelerate volumetric CEST acquisitions. Obtaining baseline measurements prior to starting chemoradiation or surgery would be valuable for ascertaining the underlying causes of CEST signal differences. There could have been imperfect estimation of the CEST

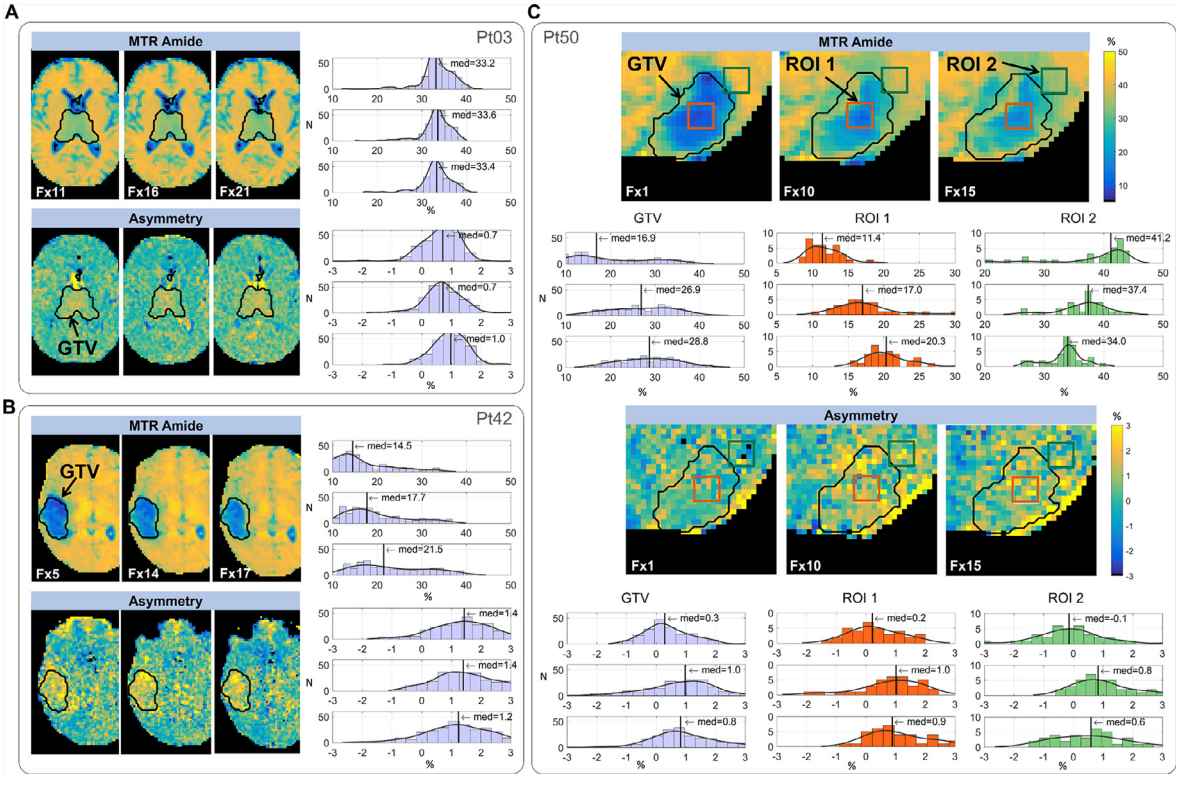

Fig. 4. CEST signal changes over time: Maps with histograms over the GTV region across treatment fractions are shown for three GBM patients. The fraction number is denoted by "Fx". (A) An example is shown of a case (Pt03) where the signals stayed relatively constant over time. (B) In Pt42, there was an increasing MTR_{Amide} signal whereas asymmetry remained relatively constant across treatment fractions. (C) In this patient (Pt50), significant changes were found in MTR_{Amide}. Increasing values were detected in ROI 1 within the GTV, whereas decreasing values were found in ROI 2, outside of the GTV. Asymmetry changes can be detected relative to the first time point.

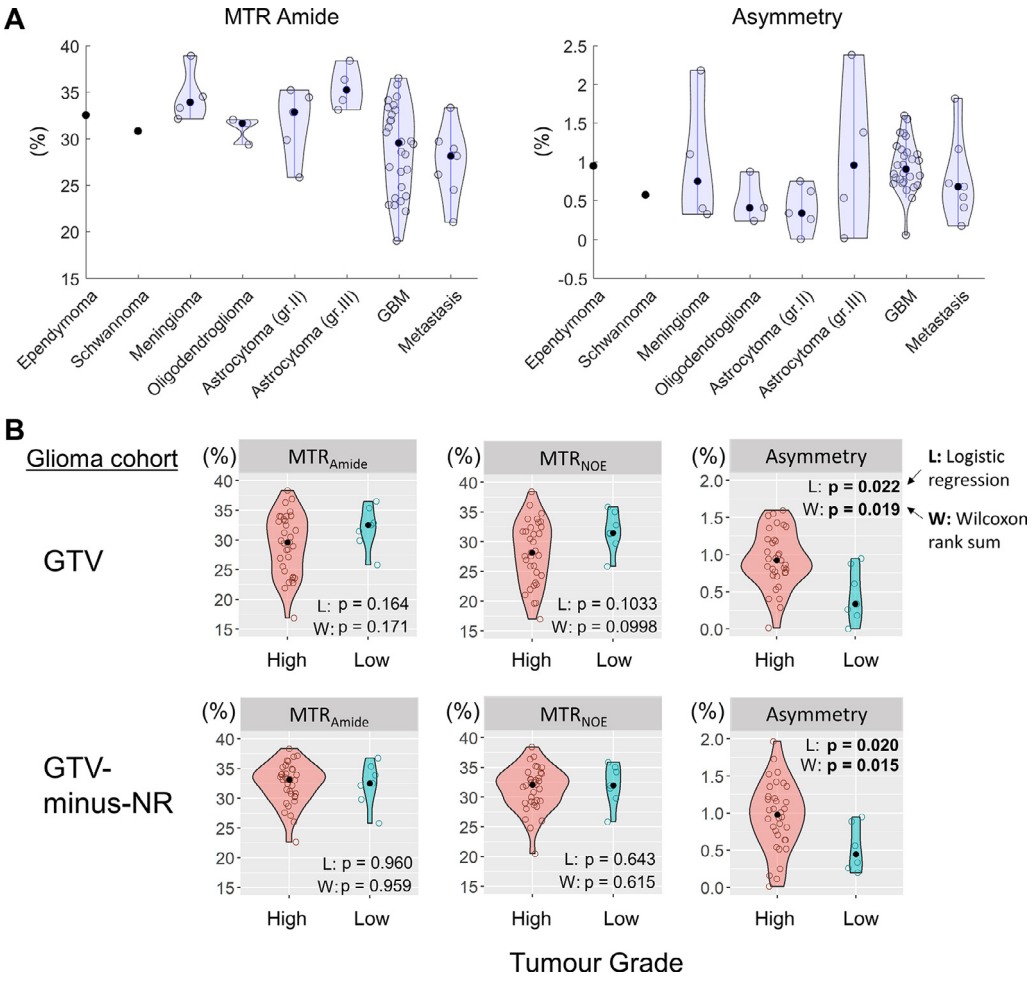

Fig. 5. CEST signals across tumour types and grades: (A) Plots of the MTR_{Amide} and asymmetry values are shown for the disease categories included in this analysis. Grades II and III astrocytomas are plotted in separate categories. One astrocytoma was omitted, as it had unknown grade due to radiological diagnosis. The ependymoma and schwannoma categories each had one case. (B) Violin plots of the high (WHO grades III and IV) and low grade (I and II) lesions are shown for each ROI, GTV and GTV-minus-NR (representing the GTV without the necrotic regions or resection cavities), and each CEST parameter. Two p-values, from the univariable logistic regression (L) and Wilcoxon rank-sum tests (W), are reported. Bolded p-values represent significance ($p < 0.05$) without correction for multiple testing.

slice locations, for example, in the 2D-to-3D registration step to register the CEST slice to the T_1-weighted volume within the same session (using mutual information as a metric). While both translations and rotations were computed between sessions (using 3D registration of the T_1-weighted images), it was assumed in the 2D-to-3D registration that there was only translation in the SI direction between the CEST slice and T_1-weighted volume within the session.

Another limitation in this study is that there was no correction for T_1, T_2, or magnetization transfer (MT) signal contributions to the observed CEST signal. The parameters assessed (in particular, the MTR_{Amide} and MTR_{NOE}) are influenced by T_1, T_2, MT and the direct saturation effect. MT would result in higher MTR_{Amide} and MTR_{NOE} values than if there were only a pure CEST effect. Some effects that are symmetric about the water peak in the z-spectra (including MT or direct saturation) are removed in the semi-quantitative CEST asymmetry metric. A direction for future analysis would be to use relaxation-compensated CEST metrics (e.g., AREX [48] or other methods [49,50]) to minimize T_1 and other non-CEST contributions to the observed CEST signal. This would be possible by incorporating into our analysis the quantitative T_1, T_2, MT data acquired on separate days as part of our larger multi-parametric imaging protocol [32]. CEST parameters within the GTVs were used, but quantification in tumour ROIs that have more spatially homogeneous signals (e.g., in core, peripheral or FLAIR hyperintense regions) can be considered [28,41,51,52]. Correlations of the CEST signal with tumour volume [53] and CEST signal variation across tumours need to be further investigated. The variations could depend on tumour location, surgical resection status and genetic subtypes (including O^6-methylguanine-DNA-methyltransferase (MGMT) methylation status, isocitrate dehydrogenase (IDH) mutation status). Clinical factors could additionally be included in a predictive model when clinical outcome data become available.

The reason for exploring the use of CEST MRI on the MR-Linac is to monitor tumour response to radiation treatment. This application is supported by previous studies [16–18,28] for assessing response to chemoradiation, and other studies showing CEST to be sensitive to changes in tumour metabolism, including the levels of mobile proteins or pH [34,54,55]. If CEST signals detected during radiation could reveal areas of residual active tumour or areas of increased tumour metabolism, then alternative treatment strategies including CEST image-guided dose escalation [12] could be applied on the MR-Linac.

Conclusions

In vivo CEST imaging of brain tumours on a clinical 1.5 T MR-Linac system is feasible within the routine clinical workflow.

Preliminary results in 54 patients demonstrated significant CEST signal contrast between tumour and cNAWM. Cohort signal changes over treatment fractions in amide/NOE MTR and changes in individual patients over time could be detected. There were differences in the CEST asymmetry signal between high- and low-grade tumours. Differences in the MTR_{Amide} and MTR_{NOE} between high- and low-grade tumours were driven by the necrotic regions or resection cavities. Our findings show that CEST holds promise for obtaining metabolic information on the MR-Linac throughout radiotherapy and may aid in treatment monitoring. Correlation with clinical outcomes will be required to determine the suitability for radiation treatment guidance.

Funding

Natural Sciences and Engineering Research Council of Canada (NSERC) (RGPIN-2017-06596, CRD 507521-16); Terry Fox Research Institute (TFRI project 1034; New Frontiers Program Project Grant); Canadian Institutes of Health Research (CIHR 156252, 148660); and Canadian Cancer Society Research Institute (CCSRI 701640, CCSRI 705083).

Acknowledgements

We thank the MR-Linac radiation therapists Shawn Binda, Danny Yu, Katie Wong, Helen Su, Monica Foster, Rebekah Shin, Khang Vo, Ruby Bola, Susana Sabaratram, Christina Silverson and Anne Carty for scanning and for their assistance with the protocol. We also thank Aimee Chan for assistance with ROIs and Wilfred Lam for useful advice.

Appendix A. Supplementary data

Supplementary data to this article can be found online at https://doi.org/10.1016/j.radonc.2021.07.010.

References

[1] Hall WA, Paulson ES, van der Heide UA, Fuller CD, Raaymakers BW, Lagendijk JJW, et al. The transformation of radiation oncology using real-time magnetic resonance guidance: A review. Eur J Cancer 2019;122:42–52. https://doi.org/10.1016/j.ejca.2019.07.021.

[2] Mutic S, Dempsey JF. The ViewRay System: magnetic resonance-guided and controlled radiotherapy. Semin Radiat Oncol 2014;24:196–9. https://doi.org/10.1016/j.semradonc.2014.02.008.

[3] Raaymakers BW, Jürgenliemk-Schulz IM, Bol GH, Glitzner M, Kotte ANTJ, Van Asselen B, et al. First patients treated with a 1.5 T MRI-Linac: Clinical proof of concept of a high-precision, high-field MRI guided radiotherapy treatment. Phys Med Biol 2017;62:L41–50. https://doi.org/10.1088/1361-6560/aa9517.

[4] Lagendijk JJW, Raaymakers BW, van Vulpen M. The magnetic resonance imaging-Linac system. Semin Radiat Oncol 2014;24:207–9. https://doi.org/10.1016/j.semradonc.2014.02.009.

[5] Winkel D, Bol GH, Kroon PS, van Asselen B, Hackett SS, Werensteijn-Honingh AM, et al. Adaptive radiotherapy: The Elekta Unity MR-linac concept. Clin Transl Radiat Oncol 2019;18:54–9. https://doi.org/10.1016/j.ctro.2019.04.001.

[6] Cao Y, Tseng CL, Balter JM, Teng F, Parmar HA, Sahgal A. MR-guided radiation therapy: transformative technology and its role in the central nervous system. Neuro Oncol 2017;19:ii16–29. 10.1093/neuonc/nox006.

[7] Dunlop A, Mitchell A, Tree A, Barnes H, Bower L, Chick J, et al. Daily adaptive radiotherapy for patients with prostate cancer using a high field MR-linac: Initial clinical experiences and assessment of delivered doses compared to a C-arm linac. Clin Transl Radiat Oncol 2020;23:35–42. https://doi.org/10.1016/j.ctro.2020.04.011.

[8] Otazo R, Lambin P, Pignol JP, Ladd ME, Schlemmer HP, Baumann M, et al. MRI-guided radiation therapy: an emerging paradigm in adaptive radiation oncology. Radiology 2021;298:248–60. https://doi.org/10.1148/radiol.2020202747.

[9] Acharya S, Fischer-Valuck BW, Kashani R, Parikh P, Yang D, Zhao T, et al. Online magnetic resonance image guided adaptive radiation therapy: first clinical applications. Int J Radiat Oncol Biol Phys 2016;94:394–403. https://doi.org/10.1016/j.ijrobp.2015.10.015.

[10] Kooreman ES, van Houdt PJ, Keesman R, Pos FJ, van Pelt VWJ, Nowee ME, et al. ADC measurements on the Unity MR-linac – A recommendation on behalf of the Elekta Unity MR-linac consortium. Radiother Oncol 2020;153:106–13. https://doi.org/10.1016/j.radonc.2020.09.046.

[11] van Houdt PJ, Yang Y, van der Heide UA. Quantitative magnetic resonance imaging for biological image-guided adaptive radiotherapy. Front Oncol 2021;10:1–9. https://doi.org/10.3389/fonc.2020.615643.

[12] Kim MM, Sun Y, Aryal MP, Parmar H, Piert M, Rosen BS, et al. A phase II study of dose-intensified chemoradiation using biologically-based target volume definition in patients with newly diagnosed glioblastoma. Int J Radiat Oncol 2020;108:S20. https://doi.org/10.1016/j.ijrobp.2020.07.2105.

[13] Wolff SD, Balaban RS. NMR imaging of labile proton exchange. J Magn Reson 1990;86:164–9. https://doi.org/10.1016/0022-2364(90)90220-4.

[14] Zhou J, Lal B, Wilson DA, Laterra J, van Zijl PCM. Amide proton transfer (APT) contrast for imaging of brain tumors. Magn Reson Med 2003;50:1120–6. https://doi.org/10.1002/mrm.10651.

[15] Jones CK, Schlosser MJ, van Zijl PCM, Pomper MG, Golay X, Zhou J. Amide proton transfer imaging of human brain tumors at 3T. Magn Reson Med 2006;56:585–92. https://doi.org/10.1002/mrm.20989.

[16] Mehrabian H, Myrehaug S, Soliman H, Sahgal A, Stanisz GJ. Evaluation of glioblastoma response to therapy with chemical exchange saturation transfer. Int J Radiat Oncol Biol Phys 2018;101:713–23. https://doi.org/10.1016/j.ijrobp.2018.03.057.

[17] Regnery S, Adeberg S, Dreher C, Oberhollenzer J, Meissner JE, Goerke S, et al. Chemical exchange saturation transfer MRI serves as predictor of early progression in glioblastoma patients. Oncotarget 2018;9:28772–83. 10.18632/oncotarget.25594.

[18] Meissner JE, Korzowski A, Regnery S, Goerke S, Breitling J, Floca RO, et al. Early response assessment of glioma patients to definitive chemoradiotherapy using chemical exchange saturation transfer imaging at 7 T. J Magn Reson Imaging 2019;50:1268–77. https://doi.org/10.1002/jmri.26702.

[19] Togao O, Yoshiura T, Keupp J, Hiwatashi A, Yamashita K, Kikuchi K, et al. Amide proton transfer imaging of adult diffuse gliomas: correlation with histopathological grades. Neuro Oncol 2014;16:441–8. https://doi.org/10.1093/neuonc/not158.

[20] Jiang S, Zou T, Eberhart CG, Villalobos MAV, Heo H-Y, Zhang Y, et al. Predicting IDH mutation status in grade II gliomas using amide proton transfer-weighted (APTw) MRI. Magn Reson Med 2017;78:1100–9. https://doi.org/10.1002/mrm.26820.

[21] Paech D, Dreher C, Regnery S, Meissner JE, Goerke S, Windschuh J, et al. Relaxation-compensated amide proton transfer (APT) MRI signal intensity is associated with survival and progression in high-grade glioma patients. Eur Radiol 2019;29:4957–67. https://doi.org/10.1007/s00330-019-06066-2.

[22] Joo B, Han K, Choi YS, Lee S-K, Ahn SS, Chang JH, et al. Amide proton transfer imaging for differentiation of benign and atypical meningiomas. Eur Radiol 2018;28:331–9. https://doi.org/10.1007/s00330-017-4962-1.

[23] Mehrabian H, Desmond KL, Soliman H, Sahgal A, Stanisz GJ. Differentiation between radiation necrosis and tumor progression using chemical exchange saturation transfer. Clin Cancer Res 2017;23:3667–75. https://doi.org/10.1158/1078-0432.CCR-16-2265.

[24] Ma B, Blakeley JO, Hong X, Zhang H, Jiang S, Blair L, et al. Applying amide proton transfer-weighted MRI to distinguish pseudoprogression from true progression in malignant gliomas. J Magn Reson Imaging 2016;44:456–62. https://doi.org/10.1002/jmri.25159.

[25] Paech D, Zaiss M, Meissner JE, Windschuh J, Wiestler B, Bachert P, et al. Nuclear overhauser enhancement mediated chemical exchange saturation transfer imaging at 7 tesla in glioblastoma patients. PLoS ONE 2014;9:3–9. https://doi.org/10.1371/journal.pone.0104181.

[26] Zaiss M, Windschuh J, Goerke S, Paech D, Meissner JE, Burth S, et al. Downfield-NOE-suppressed amide-CEST-MRI at 7 Tesla provides a unique contrast in human glioblastoma. Magn Reson Med 2017;77:196–208. https://doi.org/10.1002/mrm.26100.

[27] Chan RW, Myrehaug S, Stanisz GJ, Sahgal A, Lau AZ. Quantification of pulsed saturation transfer at 1.5T and 3T. Magn Reson Med 2019;82:1684–99. https://doi.org/10.1002/mrm.27856.

[28] Chan RW, Chen H, Myrehaug S, Atenafu EG, Stanisz GJ, Stewart J, et al. Quantitative CEST and MT at 1.5T for monitoring treatment response in glioblastoma: early and late tumor progression during chemoradiation. J Neurooncol 2021;151:267–78. https://doi.org/10.1007/s11060-020-03661-y.

[29] de Mol van Otterloo SR, Christodouleas JP, Blezer ELA, Akhiat H, Brown K, Choudhury A, Eggert D, et al. The MOMENTUM study: An international registry for the evidence-based introduction of MR-guided adaptive therapy. Front Oncol 2020;10:1328.

[30] Hoogcarspel SJ, Zijlema SE, Tijssen RHN, Kerkmeijer LGW, Jürgenliemk-Schulz IM, Lagendijk JJW, et al. Characterization of the first RF coil dedicated to 1.5 T MR guided radiotherapy. Phys Med Biol 2018;63:025014. 10.1088/1361-6560/aaa303.

[31] Keller BM, Campbell M, Ruschin ME, Kim A, McCann C, Lau A, et al. MR-Linac radiotherapy in year one: experience's in imaging, patient treatment and data collection. Int J Radiat Oncol 2020;108:e249–50. https://doi.org/10.1016/j.ijrobp.2020.07.602.

[32] Chan RW, Lawrence LSP, Oglesby RT, Chen H, Keller B, Stewart J, et al. A daily quantitative brain MRI protocol for the 1.5 T MR-Linac: feasibility of CEST with preliminary results on a prospective imaging study. Proceedings of the ISMRM & SMRT Virtual Annual Meeting & Exhibition, 2021.

[33] Jenkinson M, Beckmann CF, Behrens TEJ, Woolrich MW, Smith SM. FSL. Neuroimage 2012;62:782–90. https://doi.org/10.1016/j.neuroimage.2011.09.015.

[34] Zhou J, Heo HY, Knutsson L, van Zijl PCM, Jiang S. APT-weighted MRI: techniques, current neuro applications, and challenging issues. J Magn Reson Imaging 2019;50():347–64. https://doi.org/10.1002/jmri.26645.
[35] Jones KM, Pollard AC, Pagel MD. Clinical applications of chemical exchange saturation transfer (CEST) MRI. J Magn Reson Imaging 2018;47:11–27. https://doi.org/10.1002/jmri.25838.
[36] Choi YS, Ahn SS, Lee S-K, Chang JH, Kang S-G, Kim SH, et al. Amide proton transfer imaging to discriminate between low- and high-grade gliomas: added value to apparent diffusion coefficient and relative cerebral blood volume. Eur Radiol 2017;27:3181–9. https://doi.org/10.1007/s00330-017-4732-0.
[37] Desmond KL, Mehrabian H, Chavez S, Sahgal A, Soliman H, Rola R, et al. Chemical exchange saturation transfer for predicting response to stereotactic radiosurgery in human brain metastasis. Magn Reson Med 2017;78:1110–20. https://doi.org/10.1002/mrm.26470.
[38] Mehrabian H, Lam WW, Myrehaug S, Sahgal A, Stanisz GJ. Glioblastoma (GBM) effects on quantitative MRI of contralateral normal appearing white matter. J Neurooncol 2018;139:97–106. https://doi.org/10.1007/s11060-018-2846-0.
[39] Hong X, Liu L, Wang M, Ding K, Fan Y, Ma B, et al. Quantitative multiparametric MRI assessment of glioma response to radiotherapy in a rat model. Neuro Oncol 2014;16:856–67. https://doi.org/10.1093/neuonc/not245.
[40] Sagiyama K, Mashimo T, Togao O, Vemireddy V, Hatanpaa KJ, Maher EA, et al. In vivo chemical exchange saturation transfer imaging allows early detection of a therapeutic response in glioblastoma. Proc Natl Acad Sci 2014;111:4542–7. https://doi.org/10.1073/pnas.1323855111.
[41] Jabehdar Maralani P, Myrehaug S, Mehrabian H, Chan AKM, Wintermark M, Heyn C, et al. Intravoxel incoherent motion (IVIM) modeling of diffusion MRI during chemoradiation predicts therapeutic response in IDH wildtype glioblastoma. Radiother Oncol 2021;156:258–65. https://doi.org/10.1016/j.radonc.2020.12.037.
[42] Watanabe M, Tanaka R, Takeda N. Magnetic resonance imaging and histopathology of cerebral gliomas. Neuroradiology 1992;34:463–9. https://doi.org/10.1007/BF00598951.
[43] Jones CK, Polders D, Hua J, Zhu H, Hoogduin HJ, Zhou J, et al. In vivo three-dimensional whole-brain pulsed steady-state chemical exchange saturation transfer at 7 T. Magn Reson Med 2012;67:1579–89. https://doi.org/10.1002/mrm.23141.
[44] Zhu H, Jones CK, van Zijl PCM, Barker PB, Zhou J. Fast 3D chemical exchange saturation transfer (CEST) imaging of the human brain. Magn Reson Med 2010;64:638–44. https://doi.org/10.1002/mrm.22546.
[45] Mueller S, Stirnberg R, Akbey S, Ehses P, Scheffler K, Stöcker T, et al. Whole brain snapshot CEST at 3T using 3D-EPI: aiming for speed, volume, and homogeneity. Magn Reson Med 2020;84:2469–83. https://doi.org/10.1002/mrm.28298.
[46] Zaiss M, Ehses P, Scheffler K. Snapshot-CEST: Optimizing spiral-centric-reordered gradient echo acquisition for fast and robust 3D CEST MRI at 9.4 T. NMR Biomed 2018;31:e3879. 10.1002/nbm.3879.
[47] Zijlema SE, Tijssen RHN, Malkov VN, van Dijk L, Hackett SL, Kok JGM, et al. Design and feasibility of a flexible, on-body, high impedance coil receive array for a 1.5 T MR-linac. Phys Med Biol 2019;64:185004. 10.1088/1361-6560/ab37a8.
[48] Zaiss M, Windschuh J, Paech D, Meissner JE, Burth S, Schmitt B, et al. Relaxation-compensated CEST-MRI of the human brain at 7T: Unbiased insight into NOE and amide signal changes in human glioblastoma. Neuroimage 2015;112:180–8. https://doi.org/10.1016/j.neuroimage.2015.02.040.
[49] Heo HY, Zhang Y, Lee DH, Hong X, Zhou J. Quantitative assessment of amide proton transfer (APT) and nuclear overhauser enhancement (NOE) imaging with extrapolated semi-solid magnetization transfer reference (EMR) signals: Application to a rat glioma model at 4.7 tesla. Magn Reson Med 2016;75:137–49. https://doi.org/10.1002/mrm.25581.
[50] Lam WW, Oakden W, Murray L, Klein J, Iorio C, Screaton RA, et al. Differentiation of normal and radioresistant prostate cancer xenografts using magnetization transfer-prepared MRI. Sci Rep 2018;8:6–15. https://doi.org/10.1038/s41598-018-28731-0.
[51] Tseng C-L, Stewart J, Whitfield G, Verhoeff JJC, Bovi J, Soliman H, et al. Glioma consensus contouring recommendations from a MR-Linac International Consortium Research Group and evaluation of a CT-MRI and MRI-only workflow. J Neurooncol 2020;149:305–14. https://doi.org/10.1007/s11060-020-03605-6.
[52] Mouraviev A, Detsky J, Sahgal A, Ruschin M, Lee YK, Karam I, et al. Use of radiomics for the prediction of local control of brain metastases after stereotactic radiosurgery. Neuro Oncol 2020;22:797–805. https://doi.org/10.1093/neuonc/noaa007.
[53] Stewart J, Sahgal A, Lee Y, Soliman H, Tseng C-L, Detsky J, et al. Quantitating interfraction target dynamics during concurrent chemoradiation for glioblastoma: a prospective serial imaging study. Int J Radiat Oncol 2021;109:736–46. https://doi.org/10.1016/j.ijrobp.2020.10.002.
[54] Yao J, Tan CHP, Schlossman J, Chakhoyan A, Raymond C, Pope WB, et al. pH-weighted amine chemical exchange saturation transfer echoplanar imaging (CEST-EPI) as a potential early biomarker for bevacizumab failure in recurrent glioblastoma. J Neurooncol 2019;142:587–95. https://doi.org/10.1007/s11060-019-03132-z.
[55] Ray KJ, Simard MA, Larkin JR, Coates J, Kinchesh P, Smart SC, et al. Tumor pH and protein concentration contribute to the signal of amide proton transfer magnetic resonance imaging. Cancer Res 2019;79:1343–52. https://doi.org/10.1158/0008-5472.CAN-18-2168.
[56] Isensee F, Schell M, Pflueger I, Brugnara G, Bonekamp D, Neuberger U, et al. Automated brain extraction of multisequence MRI using artificial neural networks. Human brain mapping 2019;40(17):4952–64. https://doi.org/10.1002/hbm.24750.